An Outdoor Navigation System Using GPS and Inertial Platform

Stefano Panzieri, *Associate Member, IEEE*, Federica Pascucci, and Giovanni Ulivi, *Member, IEEE*

***Abstract*—The use of global positioning system (GPS) in outdoor localization is quite a common solution in large environments where no other reference is available and there are not so demanding positioning requirements. Of course, fine motion without the use of an expensive differential device is not an easy task, even now that available precision has been greatly improved as the military encoding has been removed. In this paper we present a localization algorithm based on Kalman filtering that tries to fuse information coming from an inexpensive single GPS with inertial data and map-based data. The algorithm is able to produce an estimated configuration for the robot that can be successfully fed back in a navigation system. Some experiments show difficulties and possible solutions of this sensor fusion problem.**

***Index Terms*—GPS, localization, outdoor mobile robotics.**

I. Introduction

OUTDOOR navigation is an exciting and quite varied topic; there are several types of environment that require different levels of autonomy and different kind of sensors. A vehicle traveling in a wood shows requirements that are not needed by one exploring a parking lot; both, however, are doing outdoor navigation. In this paper we shall address the latter situation that seems to be more promising for applications. Surveillance, cleaning, moving goods and even searching for a specific item (a car, a container) are operations that can be, in a near future, assigned to outdoor robots. By the way, such units could be freed from the usual energy shortage, because they can adopt fuel instead of batteries as the primary power supply.

Even in this rather simple environment, problems are very different from those encountered in indoor navigation; indeed, the required sensors must be different; as an example, ultrasonic sensors cannot be used, being them affected by rain and wind and having them, anyway, too short a range. However, the greatest difference is the kind of *a priori* knowledge that can be used for localization (e.g., walls and corners), a skill required also outdoors. Indeed, the typical environment features used indoors are quite scarce outdoors, moreover, large, stationary obstacles can appear and disappear: consider, e.g., the effect of some cars parked in front of a wall. When perceived by the exteroceptive sensors, they can either be interpreted as the wall itself (and therefore produce an erroneous localization) or cause the distance measures to be discarded (so reducing the amount of available information).

Outdoors, the global position system (GPS) is an interesting possibility to augment the information without adding special devices as reflectors or artificial landmarks. Until May 2000, the available precision was downgraded for military reasons, so that only differential receivers could be used for localization in the considered environments; now the full satellite precision can be achieved with a simple, cheap unit. It requires very little data processing and its error is independent of the traveled distance and from the positions of the obstacles. The problem is, therefore, to characterize the performance of this system in different situations and to adapt the localization and the navigation systems to get the maximum benefits from its use.

The paper is devoted to analyzing the localization system implemented for an ATRV-Jr. unit that moves in a parking lot on a paved but rather rugged terrain. After a brief description of the available exteroceptive sensors, the accuracy of the GPS is discussed in some detail on the basis of some experiments. Indeed, this is the most important sensor for large movements in open spaces, when no other reference is available and its short-term error affects the implementation of the entire navigation system. Other sensors, as the inertial platform and the laser scanner carried on the robot, are also examined. Their performances are presented and discussed separately.

The localization system is based on an extended Kalman filter (EKF) and it is described giving emphasis to the peculiarities arising from the characteristics of the used sensors. Finally, some guidelines are given to design the planner according to the EKF achievable performance and the nature of the environment. The description of a few experimental results concludes the paper.

II. Performance of a Simple GPS System

A GPS receiver relies on the signals, *pseudoranges*, received from several satellites that are not geostationary. Knowing the georeferenced (absolute) satellite positions from the sent messages, the antenna position and the GPS system time can be calculated if four or more pseudoranges are available.

The receiver, indeed, determines the delays along the paths from the satellites and its antenna and therefore the ranges to the satellites. The measurement process is corrupted by noise and unmodeled phenomena. These include ionospheric aberrations and unmodeled delays in the electronics. Moreover, the number and the position of the available satellites change over time influencing the system precision.

Manuscript received October 2, 2001; revised January 25, 2002. Recommended by Guest Editor B. Siciliano. This work was supported in part by the Ministry of University Scientific and Technological Research (MURST) inside the RAMSETE project.

S. Panzieri and G. Ulivi are with the Dipartimento di Informatica e Automazione, Università degli Studi "Roma Tre," 00146 Roma, Italy (e-mail: panzieri@uniroma3.it; ulivi@uniroma3.it).

F. Pascucci is with the Dipartimento di Informatica e Sistemistica, Università degli Studi "La Sapienza," 00184 Roma, Italy (e-mail: pascucci@dia.uniroma3.it).

Publisher Item Identifier S 1083-4435(02)05517-5.

TABLE I
SPECIFICATION OF GPS35-HVS

Performance	
Update Rate	1 Hz
Start up Time Valid Data	15 sec (all data known) 45 sec (initial position, time, and almanac known, ephemeris unknown) 5 min (almanac known, initial position and time unknown) 5 min (no data known)
Outputs	Position, velocity and time Receiver and satellite status Geometry and error estimate
Accuracy	
Differential GPS	5 m RMS
Non Differential GPS	15 m RMS (100 m with SA)
Environment	
Operating temperature	-40 ÷ +80 C
Electrical	
Input Voltage	6 ÷ 40 VDC
Input Current	80 mA
Backup power	Internal rechargeable 3V Li coin cell battery
Physical	
Size	5.64 × 9.63 × 2.67 cm
Weight	110 g

To estimate the position using all available satellites and the accuracy of the measures, even inexpensive GPS receivers process the pseudoranges with recursive least-square estimation techniques (i.e., KF). Therefore, a GPS receiver is also able to provide values that characterize the measurement precision, as dilution of precision (DOP) values and EPE. The DOP values are error multipliers, that indicate how the accuracy of the position estimate changes with the number and the geometry of the available satellites. Since DOP does not take into account delays in the wave propagation, it cannot be used alone as an exact measure of the localization quality. So GPS receivers often use other accuracy indicators generally called estimated position error (EPE). They are computed using statistical information from the proprietary filter used in the receiver and therefore there is no general definition for EPE.

The use of least-square filters have also an influence on the way the error changes in time. These kind of filters remove fast changing errors, so the remaining one is strongly colored. A low frequency error is remarkable if absolute position is considered, but being we interested in relative position accuracy in a rather short time, this part can be neglected. Note that the map used as for navigation in the localization algorithm is not geodetically referenced and therefore absolute position is not required.

TABLE II
SATELLITE AVAILABILITY AT POINT A

Number of satellites	First acquisition	Second acquisition	Overall percentage
4	0	11	0.6
5	0	53	2.9
6	197	127	18.0
7	685	282	53.7
8	18	427	24.7

TABLE III
SATELLITE AVAILABILITY AT POINT B

Number of satellites	First acquisition	Second acquisition	Third acquisition	Overall percentage
3	180	0	0	6.6
4	401	298	121	30.3
5	319	602	697	59.9
6	0	0	82	3.0

The robot we are considering uses the GARMIN GPS35-HVS (see Table I), a complete GPS receiver with an embedded antenna. It tracks up to twelve satellites at a time while providing one second sampling time and low-power consumption. The GPS utilizes a proprietary chipset based on high level circuit integration to minimize space and power requirements. The receiver is designed to withstand heavy operating conditions and is completely water resistant. Internal memory backup allows the GPS35-HVS to retain critical data such as satellite orbital parameters, last position, date and time. The sensor can be connected to a PC via an RS-232 interface.

To understand the level of precision and the error behavior provided by an inexpensive receiver, some experiments have been conducted in the parking lot of our department. We chose two places, say points A and B; the first was far from obstacles affecting the wave propagation, the other was in a sort of corridor, delimited by two buildings. Unfortunately, we do not know the exact georeferenced position of the two points. The robot was placed still in the two points where it acquired data in different hours of the day. All acquisitions lasted 15 minutes, during which measures were collected with a sampling period of one second, resulting in 900 measures per acquisition. Tables II and III refer the satellite availability in the two points.

As it can be seen, the number of available satellites is quite different in the two points, seven being the most probable value in the open location and five in the partially covered one. Note that four satellites is the minimum number for a complete 3–D localization.

TABLE IV
STANDARD DEVIATION (m) AT POINT A

Number of satellites	First acquisition		Second acquisition	
	E-W	S-N	E-W	S-N
4	-	-	1.0	3.5
5	-	-	1.2	3.6
6	2.3	1.1	1.9	4.2
7	2.1	1.7	2.6	4.1
8	0.4	0.0	1.0	2.3
Total	2.2	1.7	2.3	4.2

TABLE V
STANDARD DEVIATION (m) AT POINT B

Number of satellites	First acquisition		Second acquisition		Third acquisition	
	E-W	S-N	E-W	S-N	E-W	S-N
3	3.8	11.4	-	-	-	-
4	2.9	7.2	2.4	1.1	2.9	3.3
5	2.0	3.2	1.9	0.7	10.0	7.6
6	-	-	-	-	0.8	0.7
Total	3.0	7.9	2.4	0.9	10.8	9.2

Tables IV and V relate to the standard deviation of the measures for each acquisition, computed according to the number of satellites and for all the measures. Observing these tables, it easy to understand that the number of satellites provides just a rough indication of the accuracy of the measures (see, in particular, row 5 of Table V). This is shown by Figs. 1 and 2, where the two acquisitions in point B are plotted with different symbols according to the number of satellites. As it can be seen in Fig. 3, there is a lack of resolution in one direction, because the available satellites are aligned. Only the addition of the sixth satellite, which probably was not aligned, allows a remarkable increase of precision, as it can be shown by the positions of the circles in Fig. 2.

Fig. 4 shows DOP (dashed line), EPE (dotted line, values expressed in meters) values and the number of the available satellites (solid line) during a single data acquisition. Both DOP and EPE values are strongly related to the satellite number. Note that EPE is always greater than the lower bound of the accuracy provided by Table I. As we shown before, these parameters provide a measure of the absolute position accuracy, so they are not suitable for the purpose of this paper. Another important point is the way the error changes in time. An easy way to look at the phenomenon is to plot the "path" of the measured position for a given number of satellites. Looking at the regular path obtained in this way (see Fig. 3) it is easily understood that successive errors are tightly related and therefore the error is strongly colored, in particular when there are few satellites.

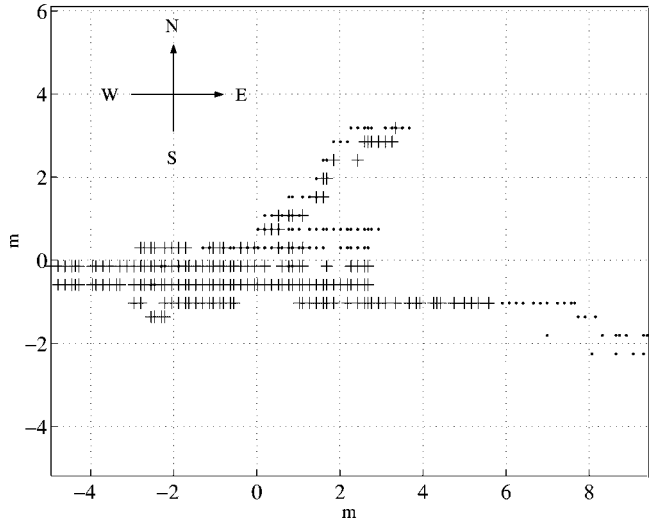

Fig. 1. Second acquisition at point B. Number of satellites: dot: 4, plus: 5.

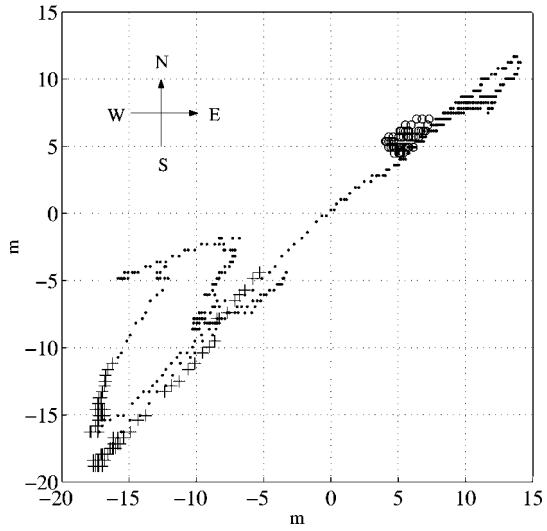

Fig. 2. Third acquisition at point B. Number of satellite: plus: 4, dot: 5, circle: 6.

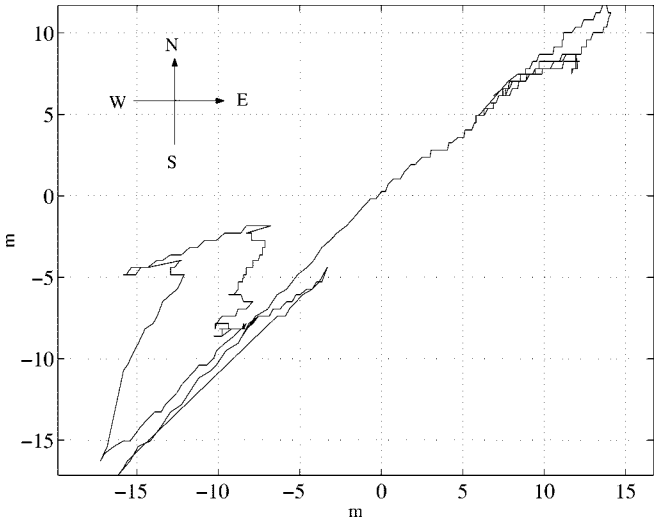

Fig. 3. Third acquisition at point B. Error path for five satellites.

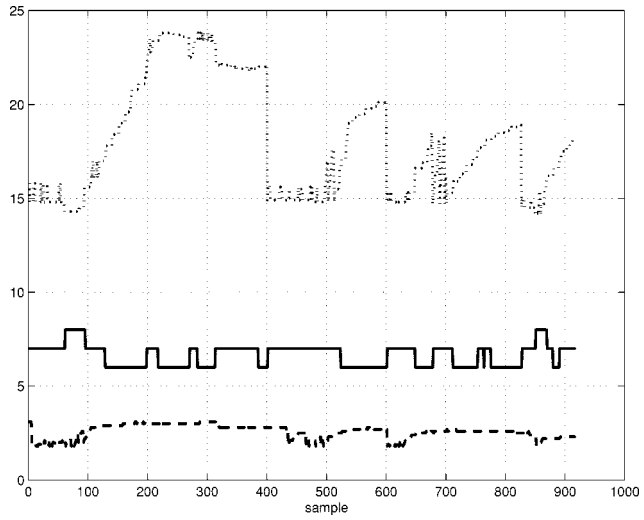

Fig. 4. DOP (dashed line), number of available satellites (solid line) and EPE (dotted line) during an acquisition at point A.

From these considerations we can conclude that EPE and the number of satellite carry, more or less, the same (small) amount of information, so we used the latter to change the covariance matrix of the GPS. Moreover, as the absolute error is slow varying, each time a known environment feature is approached, the overall error can be reset. For this reason, the localization algorithm uses the GPS subsystem as a relative sensor without requiring a strong absolute accuracy.

III. Inertial Platform

The DMU-6X (see Table VI) is a 6-DOF inertial platform designed for general measurement of linear acceleration and angular rate in dynamic environments. The DMU-6X uses a high performance digital signal processor to provide outputs that are compensated for deterministic error sources within the unit. Internal compensations include offset, scale factor and alignment. All the six DMU-6X sensing elements are solid-state devices. The three angular rate sensors are bulk micromachined vibratory MEMS sensors that utilize Coriolis force to measure angular rate independently of acceleration. The three MEMS accelerometers are surface micromachined silicon devices that use differential capacitance to sense acceleration. The DMU-6X offers both analog and digital outputs for easy system integration. Two user selectable digital output modes are provided. In scaled sensor mode, the sensor signals are sampled, converted to digital data, compensated and scaled to engineering units (g for the accelerometer and degree/second for the gyro). In voltage mode, the sensor signals are sampled and converted to digital data in voltage units. Digital data can be acquired by a PC through a serial port, while analog outputs are fully buffered and are designed to interface directly to data acquisition equipment.

TABLE VI
Specification of DMU-6X

Performance	
Update Rate	$>$ 100 Hz
Start-up Time Valid Data	$<$ 1 sec
Angular Rate	
Range: Roll, Pitch, Yaw	$\pm$ 100 deg/sec
Bias: Roll, Pitch, Yaw	$<\pm$ 100 deg/sec
Scale Factor Accuracy	$<$ 1 %
Resolution	$<$ 0.05 deg/sec
Acceleration	
Range: X,Y,Z	$\pm$ 100 G
Bias: X,Y,Z	$<\pm$ 30 mG
Scale Factor Accuracy	$<$ 1 %
Resolution	$<$ 1 mG
Environment	
Operating temperature	-40 $\div$ +85 C
Electrical	
Input Voltage	9 $\div$ 30 VDC
Input Current	$<$ 250 mA
Power Consumption	$<$ 3 W
Physical	
Size	7.62 $\times$ 9.53 $\times$ 8.13 cm
Weight	$<$ 0.59 kg

IV. LMS220 Laser Scanner

LMS220 laser scanner is a noncontact range sensor, that scans its surroundings in two dimensions. The LMS system (see Table VII) operates by measuring the time of flight of laser pulses. The pulsed laser beam is deflected by an internal rotating mirror, resulting in a fan-shaped scan. A distance value is provided every 0.25, 0.5, or 1°, depending on the angular resolution of the scanner. In this paper, we use only nine directions (referred as laser beams in the sequel). The measurement data is made available via a serial interface.

V. Localization System

We consider a mobile robot with differential drive kinematics [6], described by the following equation:

$$\begin{pmatrix} \dot{x} \\ \dot{y} \\ \dot{\theta} \end{pmatrix} = \begin{pmatrix} \cos\theta \\ \sin\theta \\ 0 \end{pmatrix} v + \begin{pmatrix} 0 \\ 0 \\ 1 \end{pmatrix} \omega. \tag{1}$$

The robot location (i.e., robot configuration [3]) is given by $x = (p^x, p^y, \phi)$, where p^x, p^y are the Cartesian coordinates of the vehicle center and ϕ is the mobile platform orientation with respect to the x axis.

The onboard sensory system includes two incremental encoders measuring the rotation of each motor, an inertial navi-

TABLE VII
SPECIFICATIONS OF LMS220

Performance	
Range	8 m / 80 m
Accuracy	5 mm (range 8 m) 10 mm (range 80 m)
Angular Resolution	0.25 / 0.5 / 1 deg
Response Time	53 / 26 / 13 ms
Electrical	
Input Voltage	24 VDC
Laser protection class	1 (eye safe)
Physical	
Weight	4.5 kg

gation system that provides measures of the robot linear accelerations and angular rates, a laser scanner which measures the distances between a fixed point on the robot body and obstacle surfaces in the environment and a GPS antenna measuring absolute position in the geodetic coordinates.

The localization system is based on an EKF in order to implement the sensor fusion.

The Kalman filter (KF), indeed, is a recursive estimator for linear system that produces the minimum variance estimate in a least squares sense under the assumption of white, Gaussian noise process. The KF also produces a measure of the accuracy of its error-state estimate, represented by the state-covariance matrix.

There are two basic process that are modeled in a KF. The first is a model describing how the state vector changes in time. This model is the system dynamic model or *system prediction*. The second model defines the relationship between the state vector and any measurement processed by the filter and is the measurement model or *observing prediction*. Intuitively, the KF sorts out information and weights the relative contribution of the measurement and of the dynamic behavior of the observing prediction. The measurements and the state vector are weighted by their respective covariance matrices. If measures are very inaccurate (large variances) with respect to the state vector estimate, then the filter will decrease the weight of measurements. On the other hand, if acquired data are very accurate (small variances) when compared to the state estimate, then the filter will tend to weigh more the measurements, with the consequence that its previous state estimate will contribute to the latest state estimate only a little.

In this paper, we use an EKF for a nonlinear system and assume that all noise sources are white Gaussian processes. A drawback in this approach is that the sources of uncertainties do not obey to a normal distribution. To partially alleviate this problem, some enhancements are used in the localization algorithm, as reported later.

The structure of the localization system, shown in Fig. 5, proceeds directly from the EKF equations [2]. At the kth step, the

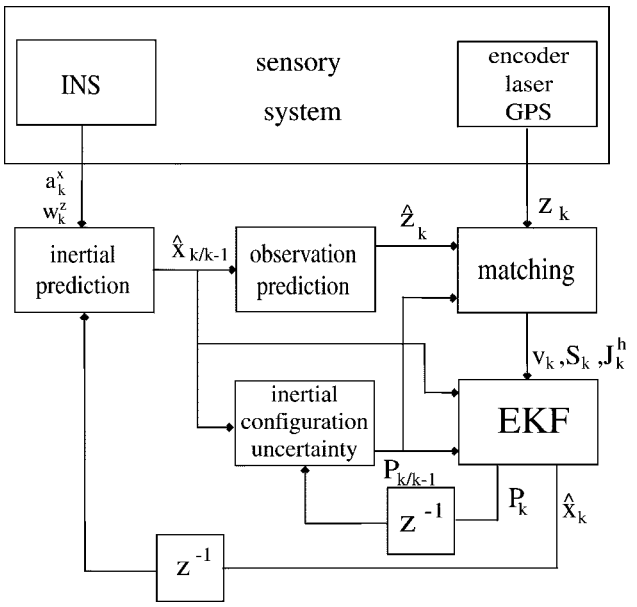

Fig. 5. Structure of the localization system (z^{-1} denotes the unit delay operator).

kinematic model of the robot is used to compute an inertial prediction $\hat{x}_{k/k-1}$ and an associated covariance matrix $P_{k/k-1}$; an observation prediction $\hat{z}_k$ is formed and compared with the measure z_k provided by the sensory system. The results are the innovation term v_k and its covariance matrix S_k, that are used by the EKF to produce the state estimate $\hat{x}_k$ and the new associated covariance P_k.

A. System Prediction

Define the state vector as $x = (p^x, p^y, \phi, v, b)$ where v is the linear velocity of the vehicle and b denotes the accelerometer bias [5]. The rate gyro bias is constant, so we estimate it only at the beginning of the navigation (see [8] for an algorithm estimating gyro bias). As stated in Section II, there is no interest in the absolute GPS position, so we avoid the introduction of a further state representing the GPS colored noise to simplify the EKF algorithm (also avoiding the risk of instability).

The inputs of the inertial model are $u_k = (a_k^x, \omega_k^z)^T$ where a_k^x is the mean robot acceleration along the motion direction and ω_k^z is the mean angular rate during the kth sampling interval. The inertial prediction is then

$$\begin{aligned}\hat{x}_{k/k-1} &= \begin{bmatrix} 1 & 0 & 0 & \Delta t_k \cos\tilde{\phi}_k & -\left(\frac{\Delta t_k^2}{2}\right)\cos\tilde{\phi}_k \\ 0 & 1 & 0 & \Delta t_k \sin\tilde{\phi}_k & -\left(\frac{\Delta t_k^2}{2}\right)\sin\tilde{\phi}_k \\ 0 & 0 & 1 & 0 & 0 \\ 0 & 0 & 0 & 1 & -\Delta t_k \cos\tilde{\phi}_k \\ 0 & 0 & 0 & 0 & 1 \end{bmatrix} \hat{x}_{k-1} \\ &\quad + \begin{bmatrix} \left(\frac{\Delta t_k^2}{2}\right)\cos\tilde{\phi}_k & 0 \\ \left(\frac{\Delta t_k^2}{2}\right)\sin\tilde{\phi}_k & 0 \\ 0 & \Delta t_k \\ \Delta t_k & 0 \\ 0 & 0 \end{bmatrix} u_k \\ &= f(\hat{x}_{k-1}, u_k, \Delta t_k) \end{aligned} \tag{2}$$

where $\tilde{\phi}_k = \phi_{k-1} + (1/2)\omega_k^z \Delta t_k$ is the average vehicle orientation during the sampling interval Δt_k. The covariance matrix associated with the prediction error is written as

$$P_{k/k-1} = J_x^f(\hat{x}_{k-1}) P_{k-1} \left(J_x^f(\hat{x}_{k-1})\right)^T + J_u^f(u_k) C \left(J_u^f(u_k)\right)^T + Q. \quad (3)$$

Here, $J_x^f(\cdot)$ and $J_u^f(\cdot)$ are the Jacobian matrices of $f(\cdot)$ with respect to $\hat{x}_{k-1}$ and u_k, P_{k-1} is the covariance matrix at time instant t_{k-1}, $C = \text{diag}\left\{\sigma_{ax}^2, \sigma_{\omega z}^2\right\}$ is the covariance matrix of the Gaussian white noise which corrupts the input measure and $Q = \text{diag}\left\{\sigma_{px}^2, \sigma_{py}^2, \sigma_{p\phi}^2, \sigma_v^2, \sigma_b^2\right\}$ is the covariance matrix of the Gaussian white noise which directly affects the state in the kinematic model.

B. Observation Prediction and Matching

The observation prediction consists of subvectors $\hat{z}_k^e$ (predicted encoder velocity), $\hat{z}_k^l$ (predicted laser readings), $\hat{z}_k^{gps}$ (predicted GPS position). For the observation prediction $\hat{z}_k^e$, we simply let

$$\hat{z}_k^e = h^e\left(x_{k/k-1}\right) = \hat{v}_{k/k-1}. \quad (4)$$

The observation prediction of the laser measures is computed over a given environment map $\mathcal{M}$ and the inertial prediction $\hat{x}_{k/k-1}$

$$\hat{z}_k^l = h^l\left(\hat{x}_{k/k-1}, \mathcal{M}\right). \quad (5)$$

It should be noted that $h^l(\cdot)$ depends on the way in which the environment map is represented—in our case, a list of segments [4]—as well as on the model interaction between the environment itself and the laser scanner. The vector $\hat{z}_k^l$ will be filled with the measured distances, each one, supposing that the ith beam detects the jth segment of the environment, can be expressed as

$$\hat{z}_{i,j}^{ls} = \frac{|a_j l_i^x + b_j l_i^y + c_j|}{|a_j \cos\vartheta_i + b_j \sin\vartheta_i|} \quad (6)$$

where (a_j, b_j, c_j) are the segment parameters while $(l_i^x, l_i^y, \vartheta_i)$ is the configuration if the ith beam. Of course some processing is required to determine which segment is affected by the reflection.

The subvector $\hat{z}_k^{gps}$ is written as

$$\hat{z}_k^{gps} = h^{gps}\left(x_{k/k-1}\right) = \left(\hat{p}_{k/k-1}^x, \hat{p}_{k/k-1}^y\right)^T. \quad (7)$$

The conversion 7 of the GPS measure from geodetic coordinates to the environment framework is based on elementary trigonometry.

The innovation term and the associated covariance, being $\hat{z}_k = \left(\hat{z}_k^e, \hat{z}_k^l, \hat{z}_k^{gps}\right)$ and z_k the measured outputs, are then computed as

$$v_k = z_k - \hat{z}_k \quad (8)$$

$$S_k = J_x^h\left(\hat{x}_{k/k-1}\right) P_{k/k-1} \left(J_x^h\left(\hat{x}_{k/k-1}\right)\right)^T + R_k \quad (9)$$

where $J_k^h(\cdot)$ is the Jacobian matrix of $h = (h^e, h^l, h^{gps})$ with respect to $x_{k/k-1}$. The first term used to compute S_k represents the uncertainty on the observation due to the uncertainty on the inertial prediction. The second term is the observation noise covariance matrix.

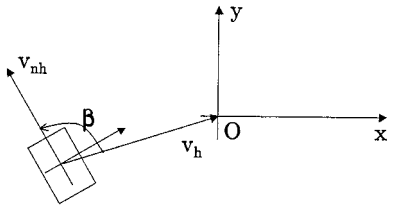

Fig. 6. Holonomic and nonholonomic velocities.

The measurement noise depends on the interaction between the sensor system and the environment, which is not invariant in space and time. For example, some surfaces (glass or hedges) are more difficult to detect for laser sensor. To model this fact, we have chosen to label each segment of the map with a value representing the reliability of the laser measure provided by that segment and to modify the correspondent rows of the covariance matrix R accordingly [7]. Also, the GPS submatrix of R are modified by the number of satellite that the antenna uses at the instant time t_k, because the sensor accuracy depend on their number and position.

Moreover, to avoid the inclusion of outliers in the correction phase, we need to set up a *validation gate* as follows for the laser measures [1]. Suppose that $v_{k,j}$ is the innovation term for a laser ray; it will be passed to the EKF only if its Mahalanobis distance satisfies the inequality

$$\frac{v_{k,j}^2}{s_j} \leq \gamma^2 \quad (10)$$

where s_j is the jth diagonal term of S and parameter γ should be tuned by experimental trials. In this way a large innovation $v_{k,j}$ is validated only if the associated covariance s_j is big enough. In addition, GPS measures obtained using less than four satellites are discharged.

C. EKF

The EKF is used to correct the inertial configuration estimate on the basis of the validated observations. In particular, the final configuration estimate is obtained as

$$\hat{x}_k = \hat{x}_{k/k-1} + K_k\left[z_k - \hat{z}_k\right] \quad (11)$$

where K_k is the Kalman gain matrix

$$K_k = P_{k/k-1}\left(J_x^h\left(\hat{x}_{k/k-1}\right)\right)^T S_k^{-1}. \quad (12)$$

The covariance associated with the final configuration estimate $\hat{x}_k$ is given by

$$P_k = P_{k/k-1} - K_k S_k K_k^T. \quad (13)$$

VI. Planning and Control

Many algorithms are available to plan a trajectory for the considered application. Here we report only some simple remarks on the specific constraints deriving by the use of the GPS. As explained before, the GPS provides the position of the robot with a maximum error that can be as high as 20 m, even if generally

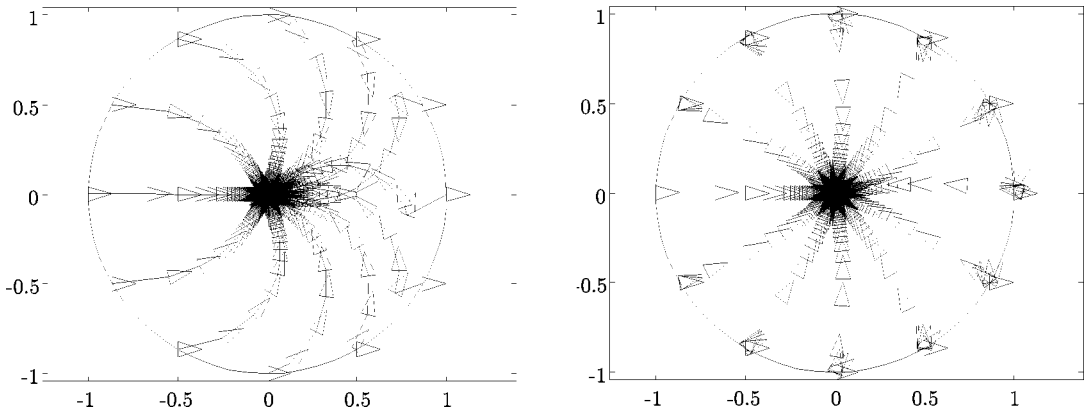

Fig. 7. Trajectories without forward cutoff (left) and with forward cutoff (right).

this is quite lower. When the trajectory proceeds for a long time far from any reference point, the position error can reach such a value. Then, if the range of the other exteroceptive sensors is larger than the position error, this can be corrected when a feature appears in the robot field of view. Otherwise, as it could happen in our case, the error cannot be corrected. This event is uncommon and its occurrence can be avoided by planning a path that passes near some environment feature before the errors grow too large, even if in this way the minimum length property is missed. Moreover, if the DOP is available, this behavior can be activated only when needed, perhaps by a real time trajectory reconfiguration.

In our implementation the user enters a sequence of properly chosen via points to describe the desired path. The robot passes from one of them to the next using a simple control algorithm based on a static time invariant feedback control law on each segment. It is well-known that, for nonholonomic systems like unicycle robots, the point tracking problem, i.e., tracking of only Cartesian coordinates, can be solved using a partial feedback linearization of the dynamic model and a simple PD like control law in the new coordinates [10]. If we suppose that both exact tracking along each segment and a particular posture at the via point are not required, the problem can be relaxed to the stabilization of only the first two coordinates of system (1). This could be attained with an easy strategy, obtained by simplifying the one presented in [11]: first of all (see Fig. 6) define a suitable holonomic velocity v_h, unaware of the nonholonomic constraint, able to perform the stabilizing task, i.e., able to steer the origin of the robot frame over the origin O of the reference frame; second, define two control laws one as projection of v_h along the nonholonomic direction v_{nh} and the other steering the nonholonomic axis of the vehicle toward the holonomic velocity vector (to reduce the angle β between the two vectors)

$$v = K_e \, \|v_h\| \cos(\beta) \tag{14a}$$

$$\omega = - K_\omega \beta. \tag{14b}$$

The convergence to the origin can be easily proved considering that (14b) independently steers the robot orientation ϕ to a value that will definitively let $\beta = 0$. Now, using a Lyapunov candidate function $V(x,y) = x^2 + y^2$ it is easy to see that its derivative is, when $\beta = 0$, $\dot{V} = -2K_e(x^2+y^2)$ and is negative defined. At the left of Fig. 7 trajectories generated for different starting points are reported. To avoid back motion a different strategy has been applied and its results reported at the right of the same figure: the first control has been set at zero until $\| \beta \|$ is less than a threshold of 10 °. In this case trajectories are more linear and therefore, this strategy has been preferred. The only point where this control fails is the origin itself (where β is undefined) but also to avoid strong discontinuities in the control law, possibly caused by sudden corrections of the estimated position due to new available laser measures, the via points have been defined as a circular region of radius 0.5 m and the robot has been forced to halt when it steps into this region.

Finally, to take into account the presence of unexpected obstacles, an obstacle avoidance module has been added [9] which provides *small* variations of the desired value of the robot orientation ϕ according to the sensor readings.

VII. Experimental Results

The proposed algorithm has been tested on the mobile robot ATRV-Jr. produced by Real World Interface (see Fig. 8). The robot has four tires, actuated by two independent motors, so the kinematic model of the platform is a differential drive one. The sensory system, described before, is connected to the ATRV-Jr. onboard PC (Pentium II, 350 MHz) through a serial port on a Rockeport multiserial port card. On the same PC run the low level control software (the RWI's ReFlex accepting speed commands and returning odometric data) and the CORBA servers, that distribute the sensor data over the network. The high level control software, written in C++ language, is a client program that runs on a notebook (Pentium II at 366 MHz) that interacts with the ATRV-Jr. using TCP/IP over an Ethernet link. The experiment here reported has been conducted in the parking lot of our department (Fig. 9). The navigation algorithm described in Section VI has been implemented using data coming from the localization filter.

The robot, starting its path in S (see Fig. 9), remains still for 15 s to estimate both the initial bias for the inertial navigation system and the offset for the GPS Cartesian position. In this figure, the odometric path (dashed) is extremely inaccurate and rapidly diverges while the GPS estimate (solid line) has a limited error. The output of the filter (circles) does not coincide with the effective path (white dashed line) but its maximum deviation has been of 0.5 m.

Fig. 8. The mobile robot ATRV-Jr.

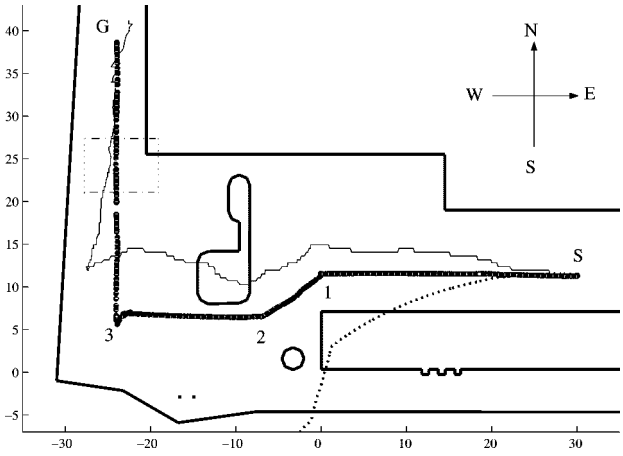

Fig. 9. Robot path in the department parking lot: the path by the algorithm (circle), GPS (solid line) and odometry (dashed line), real path (white dashed line).

After the initialization step, while moving at constant speed toward point 1, the robot integrates satellite measures with laser readings but, due to unpredictable obstacles (parked cars) the matching with the map is not always possible. Moreover, in the front direction, walls are too far (more than eight meters) and the estimated position relies only on GPS with an error that slowly increases. When the robot approaches point 1 and the laser system starts to give a reliable measure that can be matched with the map, the error is reduced from 0.4 m–0.1 m. To help the KF, an additional stop of a few seconds is used to stabilize the estimate configuration. After that, circumnavigating the obstacle, the robot moves to via points 2 and 3. Although the robot, approaching point 3, has no information from the laser system and uses only GPS data, its position estimate does not appreciably drift toward the GPS one (north); this can be explained observing the covariance matrix associated to the GPS data that is greater than position estimate covariance matrix ($P_{k/k-1}$). This dominance, with actual gains, would last only for about

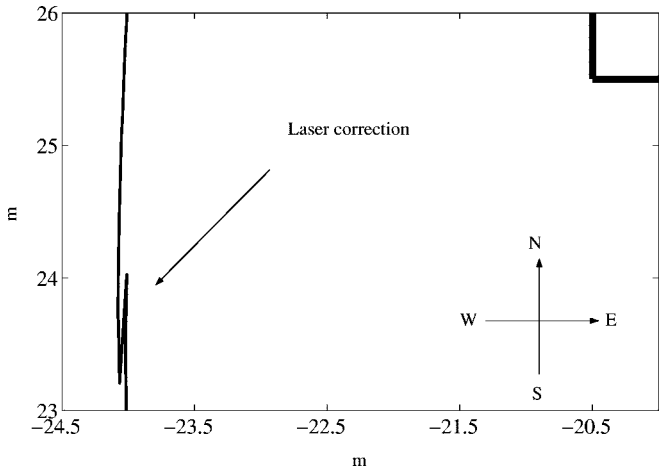

Fig. 10. Laser correction on building corner.

one minute; after this interval $P_{k/k-1}$ would degrade and the position estimate would coincide with GPS values.

In point 3, the west limit of the parking lot is seen by laser system and the longitudinal position is again accurate when the robot starts to move toward the goal G. Along this last segment a singular adjustment occurs: the particularly bad latitude estimate is suddenly fixed as the corner is recognized. In the same figure, the magnification in Fig. 10 shows the discontinuity that has a negligible effect on the control law as stated before.

VIII. Conclusion

The elimination of the selective availability from the GPS has made outdoor localization available even using inexpensive receivers. In this paper, an experimental analysis of its performance is reported and it is used, together with other sensors, to implement an EKF for an ATRV-Jr. robot. This error also affects the strategy of the planning system: if large errors are expected the trajectory must pass near some easily recognizable environment feature, even if this lengthens the path.

References

[1] J. J. Leonard and H. F. Durrant-Whyte, "Mobile robot localization by tracking geometric beacons," *IEEE Trans. Robot. Automat.*, vol. 7, pp. 376–382, June 1991.

[2] A. C. Gelb, *Applied Optimal Estimation*. Cambridge, MA: MIT Press, 1994.

[3] J. C. Latombe, *Robot Motion Planning*. Boston, MA: Kluwer, 1991.

[4] J. Gonzalez, A. Stenz, and A. Ollero, "An iconic position estimator for a 2D laser rangefinder," in *Proc. IEEE Int. Conf. Robotics and Automation*, San Diego, CA, 1992, pp. 2646–2651.

[5] B. Barshan and H. F. Durrant-Whyte, "Inertial navigation system for mobile robots," *IEEE Trans. Robot. Automat.*, vol. 7, pp. 376–382, June 1991.

[6] J. Borenstein, H. R. Everett, and L. Feng. (1996) 'Where Am I?' Sensors and Methods for Mobile Robot Positioning. Univ. Michigan, Ann Arbor. [Online]ftp://ftp.eecs.umich.edu/people/johannb/pos96rep.pdf.

[7] E. Fabrizi, G. Oriolo, S. Panzieri, and G. Ulivi, "Enhanced uncertainty modeling for robot localization," presented at the 7th Int. Symp. Robotics With Application (ISORA), Anchorage, AL, 1998.

[8] ——, "Mobile robot localization via fusion of ultrasonic and inertial sensor," presented at the 8th Int. Symp. Robotics With Application, Maui, HI, 2000.

[9] E. Fabrizi, S. Panzieri, and G. Ulivi, "An integrated sensing-guidance system for a robotized wheelchair," in *Proc. 14th IFAC World Congr.*, Beijing, China, July 5–9, 1999, pp. 457–462.
[10] B. d'Andréa-Novel, G. Champion, and G. Bastin, "Control of nonholonomic wheeled mobile robots by state feedback linearization," *Int. J. Robot. Res.*, vol. 14, pp. 543–559, 1995.
[11] M. Aicardi, G. Cannata, G. Casalino, and G. Indiveri, "On the stabilization of the unicycle model projecting a holonomic solution," presented at the Proc. 8th Int. Symp. Robotics With Application, Maui, HI, 2000.

Stefano Panzieri (S'92–M'93–A'94) was born in Rome, Italy, in 1963. He received the "Laurea" degree in electronic engineering and the Ph.D. degree in systems engineering, both from the University of Rome "La Sapienza," Rome, Italy, in 1989 and 1994, respectively.

In February 1996, he joined the Dipartimento di Informatica e Automazione (D.I.A.), University of "Roma Tre," as a Research Associate (Ricercatore), he is currently a Professor of automatic control. His research interests are in the field of industrial control systems. Several published papers concern the study of iterative learning control applied to robots with elastic elements and to nonholonomic systems. In particular, in the area of mobile robots, he studied the problem of localization in structured and unstructured environments with a special attention to the problem of sensor-based navigation.

Federica Pascucci was born in Rome, Italy, in 1975. She received the degree in engineering and specialization control systems from the University of "Roma Tre," in 2000. She is currently pursuing the Ph.D. degree at the "Dipartimento di Informatica e Sistemistica," University of Rome "La Sapienza," Rome, Italy.

Her research interests are in the field of mobile robot perception. In particular, she is dealing with the problem of mobile robot localization in (partially) known environments.

Giovanni Ulivi (M'95) was born in Rome, Italy, in 1950. He received the Laurea degree in electrical engineering from the University of Rome "La Sapienza," Rome, Italy, in 1974.

In 1974, he joined the Department of Computer and System Science, University of Rome "La Sapienza." In 1992, he joined the Department of Computer Science and Industrial Automation, University of "Roma Tre," where he currently heads the Advanced Robotics Laboratory, teaches automatic control, and is the tutor of several Ph.D. students. His research interests, begun with the control of electric motors, now include nonlinear control of rigid and elastic robots, autonomous vehicle control, and scene recognition for motion planning. He is the author of about 100 scientific papers.

Dr. Ulivi is a member of the International Federation of Automatic Control (IFAC) and participates on the technical committees of Robotics, Autonomous Vehicles, and Components and Instruments.